World Applied Sciences Journal 8 (8): 1022-1031, 2010
ISSN 1818-4952

Vibrational Analysis of Flexible Coupling by Considering Unbalance

[1]V. Hariharan and [2]P.S.S. Srinivasan

[1]Department of Mechanical Engineering, Kongu Engg College, Perundurai, Erode-638052, India
[2]Principal, Knowledge Institute of Technology, Kakapalayam, Salem, India

Abstract: Misalignment and unbalance is the most cause of machine vibration. An unbalanced rotor always cause more vibration and generates excessive force in the bearing area and reduces the life of the machine. Understanding and practicing the fundamentals of rotating shaft parameters is the first step in reducing unnecessary vibration, reducing maintenance costs and increasing machine uptime. In this paper, experimental studies were performed on a rotor dynamic test apparatus to predict the vibration spectrum for rotor unbalance. A self-designed simplified 3 pin type flexible coupling was used in the experiments. The rotor shaft accelerations were measured at four different speed using accelerometer and dual channel vibration analyzer (ADASH) under the balance (baseline) and unbalance conditions. The experimental and numerical (ANSYS) frequency spectra were also obtained for both base line and unbalanced condition under different unbalanced forces. The experimental predictions are in good agreement with the ANSYS results. Both the experimental and numerical (ANSYS) spectra show that unbalance can be characterized primarily by one times (1X) shaft running speed.

Key words: Misalignment · Unbalanced rotors · Coupling

INTRODUCTION

Rotor unbalance is the most common reason in machine vibrations. Most of the rotating machinery problem can be solved by using the rotor balancing and misalignment. Mass unbalance in a rotating system often produces excessive synchronous forces that reduce the life span of various mechanical elements. A very small amount of unbalance may cause severe problem in high speed rotating machines. Overhung rotors are used in many engineering applications like pump, fans, propellers and turbo machinery. The vibration signature of the overhung rotor is totally different from the center hung rotors. The vibration caused by unbalance may destroy critical parts of the machine, such as bearings, seals, gears and couplings. Rotor unbalance is a condition in which the centre of mass of a rotating assembly, typically the shaft and its fixed components like disks and blades etc. is not coincident with the centre of rotation. In practice, rotors can never be perfectly balanced because of manufacturing errors such as porosity in casting, non-uniform density of material, manufacturing tolerances and gain or loss of material during operation [1] As a result of mass unbalance, a centrifugal force is generated and must be reacted against by the bearings and support structures. A number of analytical methods have been applied to unbalance response such as the transfer matrix method [2], the finite element method [3] and the component mode synthesis method [4]. Unbalance response investigations of geared rotor-bearing systems, based on the finite element modeling, Neriya *et al*. [5] and Kahraman *et al*. [6] carried out investigations utilizing the modal analysis technique. Besides, based on the transfer matrix modeling, Iida *et al*. [7] and Iwatsubo *et al*. [8] reported on studies utilizing the usual procedure of solving simultaneous equations and Choi and Mau [9] utilizing the frequency branching technique. Further, concerning unbalance response investigations of dual shaft rotor-bearing systems coupled by bearings, based on the transfer matrix modeling, Hibner [10], Li *et al*. [11] and Gupta *et al*. [12] carried out investigations utilizing the usual procedure of solving simultaneous equations. However all the above investigations resulted in full numerical solutions of the unbalance responses of coupled two-shaft rotor-bearing systems. On the other hand, Rao [13] suggested analytical closed-form expressions for the major and minor axis radii of the unbalance response orbit for one-shaft rotor-bearing

Corresponding Author: V. Hariharan, Department of Mechanical Engineering,
Kongu Engg College, Perundurai, Erode-638052, India

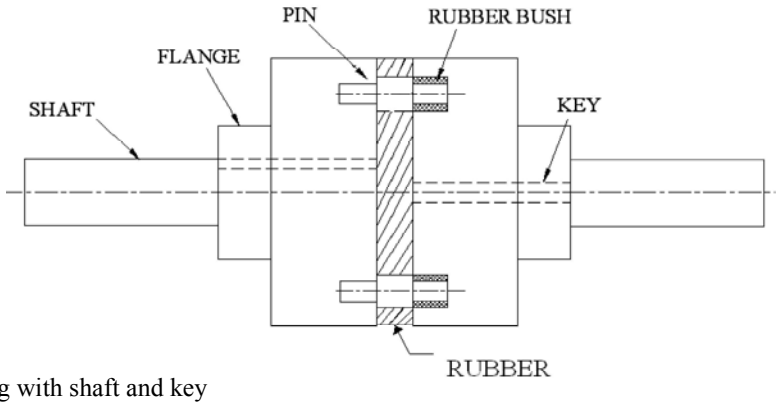

Fig. 1: Pin type coupling with shaft and key

system. Rao *et al*. [14] and Shiau *et al*. [15] investigated the lateral responses of geared rotors due to short circuit torsional excitation. In this paper a general method is presented for obtaining the unbalance response orbit based on the finite element approach of a gear-coupled two-shaft rotor-bearing system, where the shafts rotate at different speeds. Specifically, analytical solutions of the maximum and minimum radii of the orbit are proposed. In addition, the validity of the proposed analytical solutions of the orbit radii is tested against those obtained fully numerically. In this paper unbalance system of a overhung rotors are considered for unbalance study. Experiments were conducted for two different weights of masses at four different speeds and results are plotted. The rotor unbalance can be detected by spectral analysis. The vibration frequency of rotor unbalance is synchronous that is one times the shaft rotational speed (1X r.p.m.), since the unbalance can be reduced significantly by rotor balancing.

Description of Pin Type Coupling: The newly designed coupling is as shown in Figure 1. It has two flanges. One flange has a pin hole of required number at pitch circle diameter. The other flange will have a number of pins projected outside at pitch circle diameter to accommodate into the first flange holes with rubber bush. The driver and driven shafts are connected to their respective flanges i.e. output and input flanges by means of parallel square key. Mild-steel is considered for the input and output shafts, pins and keys. Over these pins, a circular natural rubber bush is provided and its length is equal to the length of the hole. The diameter of the flange holes is equal to the diameter of pin plus the thickness of rubber bush.

The cast-iron material is chosen for both left and right flanges and the natural rubber is for bush. There is no nut and bolt to clamp the both input and output flanges. The following Figure 1 represent the two dimensional model of self designed 3 pin type coupling. In between flanges a rubber material is introduced to give the flexibility. Dimensions of the coupling and materials used is given in Table 1 and Table 2.

Description of the Experimental Setup: The Experimental apparatus is shown in Figure 2 and Figure 3. It consists of a D.C. motor, a flexible coupling and a single disk rotor. The rotor shaft is supported by two identical ball bearings and has a length of 466 mm with a bearing span of 197 mm. The diameter of the rotor shaft is 19 mm. A disk of 128 mm in diameter and 7 mm in thickness is mounted on the rotor shaft non drive end. The bearing pedestals are adjustable in vertical direction so that different misalignment conditions can be created. The rotor shaft is driven by 0.75 hp D.C. motor. The D.C. voltage controller is used to adjust the power supply so that motor speed can be continuously increased or decreased in the range from 0 to 2000 rpm. Two dial gauge method is used to correct the shaft misalignment and base line signal has been measured at 4 different speeds to check the concentricity.

The instruments used in the experiments include accelerometers and dual channel vibration analyzer. The accelerometer directly measures the acceleration of bearing housing vibration and displays in the vibration analyzer.

Experimental Procedure: Experimental facility as shown in Figure 2 is used for unbalance test. First the setup is run for few minutes to settle down all minor vibrations. Before creating the unbalanced, the shaft is checked for any misalignment and unbalance. Two dial gauge method is used to check the proper alignment and balancing. After this an unbalance has been created by placing a mass of 18 gram in the overhung rotor at a radius of 54 mm. Accelerometer along with the vibration analyzer is

Table 1: Dimension of the shaft and coupling

Sl.No	Description	Unit
1	Shaft diameter	19 mm
2	Length of the Shaft	466 mm
3	Hub diameter	40 mm
4	Length of the hub	30 mm
5	Outside diameter of flange coupling and Rubber pad	80 mm
6	Number of holes for pin	3
7	Diameter of pin hole	11 mm
8	Diameter of pin	6 mm
9	Rubber bush Outside diameter	11 mm
	Inside diameter	6 mm
10	Keyway Depth	
	In shaft	3.5 mm
	In hub	2.8 mm
	Keyway cross section	
	Height	6 mm
	Width	6 mm

Table 2: Material Properties

Properties	Cast-iron	Mild steel	Rubber
Young's modulus, (MPa)	1×10^5	2×10^5	30
Poisson ratio	0.23	0.3	0.49
Density, (kg/mm^3)	7250^{-9}	7850^{-9}	1140^{-9}

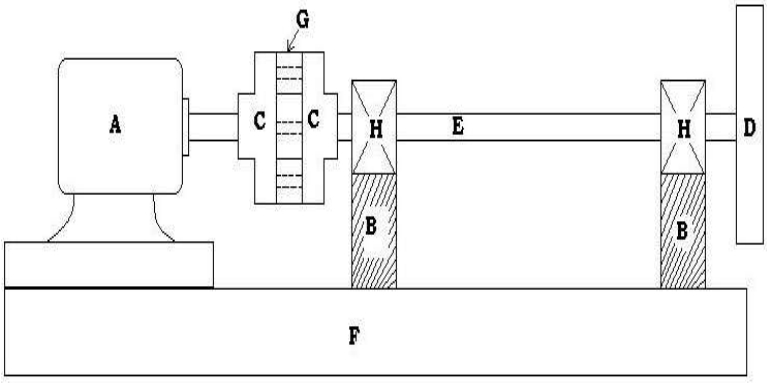

Fig. 2: Experimental set up of pin type flexible coupling
A-D.C Motor, B-Bearing Support, C-Coupling, D-Disk, E-Rotor Shaft, F-Base, G-Rubber, H-Ball Bearing

Fig. 3 Photo graph of experimental setup

used to acquire the vibration signals. The accelerometer is calibrated with the help of calibration test accelerometer fitted with the electro dynamic shaker and power amplifier under known frequency and amplitude. The acceleration amplitude of the electro dynamic shaker is compared with the acceleration amplitude of the accelerometer to be calibrated. Vibration amplitude of both the electro dynamic shaker and test accelerometer are found to be same. Calibrated accelerometer is fitted over the bearing housing and connected to the vibration analyzer. Vibration signals are measured at four different speeds 500, 1000, 1500 and 2000 rpm with the well balanced and unbalanced rotor system at both drive end (DE) and non drive end (NDE) and stored in the vibration analyzer.

Generalized System Equation of Motion: The equation of motion for the rotor can be written in partitioned form as

$$\begin{pmatrix} m^r_{11} & m^r_{1B} \\ m^r_{B1} & m^r_{BB} \end{pmatrix} \begin{bmatrix} \ddot{x}^r_1 \\ \ddot{x}^r_B \end{bmatrix} + \begin{pmatrix} k^r_{11} & k^r_{1B} \\ k^r_{B1} & k^r_{BB} \end{pmatrix} \begin{bmatrix} x^r_1 \\ x^r_B \end{bmatrix} = \begin{bmatrix} F^r_1 \\ F^r_B \end{bmatrix} \quad (3.1)$$

Where $\{x_1^r\}$ and $\{x_B^r\}$ are the interior and boundary co-ordinates of the rotor, respectively.

Two types of components of modes are used in the component mode syntheses process, namely fixed-interface normal modes and constraint modes. The normal modes of the rotor are obtained from the Eigen value equation.

$$([K_{11}]- \omega^2_{ri}[m^r_{11}])\{\phi^r_1\}_i = \{0\}, \; i=1,2\ldots, n_r \quad (3.2)$$

Where ω^2_{ri} and $\{\phi^r_1\}$ are the i th fixed-interface natural frequency and normal mode of the rotor and n_r is the number of degrees of freedom of the rotor with fixed interface.

The participation criterion is used to truncate the higher order normal modes of the components. By considering the accuracy and efficiency of the solutions, the upper frequency limit is determined to be 1000 Hz. The normal operating speed of the system study is about 160 Hz. Hence, it is almost impossible to excite those component normal modes with natural frequencies above 1000Hz in practice. For the purpose of generality, it is assumed that t_r lower modes are retained for the rotor. The truncated normal modes are written in matrix form as

$$\{\phi^r_1\} = [\{\phi^r_1\}_1, \{\phi^r_1\}_2, \ldots\ldots\ldots\{\phi^r_1\}_{tr}] \quad (3.3)$$

The constrained modes of the rotor are obtained from the static equation.

$$[K^r_{11}]\{x^r_1\}+[K^r_{1B}]\{x^r_B\}= \{0\} \quad (3.4)$$

Using the Guyan reduction technique [24], equation (3.4) becomes

$$\{x^r_1\}=[\phi^r_B]\{x^r_B\} \quad (3.5)$$

Where

$$[\phi^r_B]=-[K^r_{11}]^{-1}[K^r_{1B}] \quad (3.6)$$

The matrix $[\{\phi^r_B\}]$ contains the constraint modes of the rotor. The same procedures are also applied to the motor and flexibile coupling to obtain the truncated normal modes and constraint modes.

By using modal coordinates {p}, the generalized system equations of motions can be written as

$$[M]\{\ddot{p}\} + [K]\{p\}=\{Q\} \quad (3.7)$$

Numerical Method (Finite Element Modeling)

Modeling of the Rotor Shaft and Coupling: Rotor shaft and coupling modeled using Pro/Engineer wildfire with the exact dimensions as used in the experimental setup. The dimensions of the coupling and the material properties are shown in the Table 1 and Table 2. Material property of rubber is initially defined as an isotropic material with young's modulus and poison's ratio value. In this stage the rubber is act as linear material. To convert it in to nonlinear material hyper elastic property with Mooney Rivlin Constants is introduced. There are several Mooney Rivlin constants are available. In this analysis an accurate method of 9 constants are used. The Mooney Rivlin constants are given in the Table 3. These constants are responsible for non linear property of the natural rubber. The surface to surface contact is considered for rubber and cast iron flange.

Meshing Formulation: Before meshing the model and even before building the model, it is important to think about whether a free mesh or a mapped mesh is appropriate for the analysis. A free mesh has no restrictions in terms of element shapes and has no specified pattern applied to it. A mapped mesh is restricted in terms of the element shape it contains and the pattern of the mesh. A mapped area mesh contains either quadrilateral or triangular elements, while the mapped volume mesh contains hexahedron elements. In addition, a mapped mesh typically has a regular pattern, with obvious rows of elements. In this type of mesh, first it built the geometry as a series of fairly regular volumes and/or areas and later that can be accepted the mapped mesh.

In this model, the mapped mesh has been used with the element type of SOLID 95. Smart element size control is used for mapped mesh. SOLID95 is a higher order version of the 3D 8-noded solid element. Meshed model is shown in Figure 4.

It can tolerate irregular shapes without the loss of accuracy. SOLID95 elements have compatible displacement shapes and are well suited to model curved boundaries.

Table 3 Mooney Rivlin Constants

C_1	C_2	C_3	C_4	C_5	C_6	C_7	C_8	C_9
58.66	0.774	54.26	-117.49	52.77	3.58	-23.067	33.69	-12.486

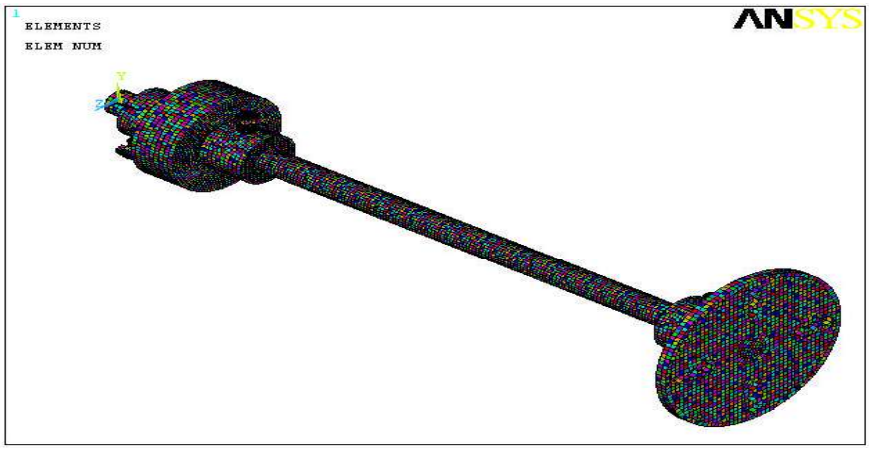

Fig. 4: Meshed rotor shaft and coupling

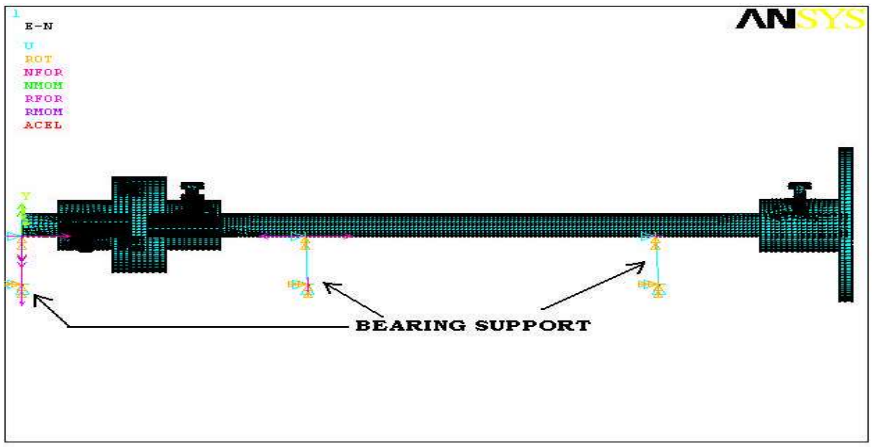

Fig. 5: Rotor systems with boundary conditions

Boundary Conditions and Loading: The rotor shaft is supported between two identical ball bearings of 197 mm span. The bearing P204 type is represented by COMBIN40 element and the stiffness of the bearing is $1.5x10^4$ N/mm. Figure 5 shows the boundary conditions.

The rotor shaft model rotates with respect to global Cartesian X-axis. The angular velocity is applied with respect to X-axis. The degree of freedom along UX, UZ, ROTY, ROTZ are fixed at bearing ends. Different angular velocities are given as input and corresponding accelerations are measured at both drive end and non drive end.

A computer program CMSP (Component Mode Synthesis Program) for the vibration analysis of a motor-flexible coupling-rotor system was developed on the basis of the theoretical model and analysis. The CMSP program was used to solve the system equations of motion for different unbalance condition. The commercial finite element package ANSYS was used for the component modeling and analysis. These results are used for evaluating the experimental results.

RESULTS AND DISCUSSION

Frequency Spectrum of Base Line Condition: The experimental and simulated frequency spectra were obtained to baseline condition. The perfect alignment and balance cannot be achieved in practice. Thus, a baseline case is presented first to show the residual unbalance and misalignment. The measured acceleration of an well aligned and balanced system at drive end (DE) and non drive end (NDE) with the self designed 3 pin type

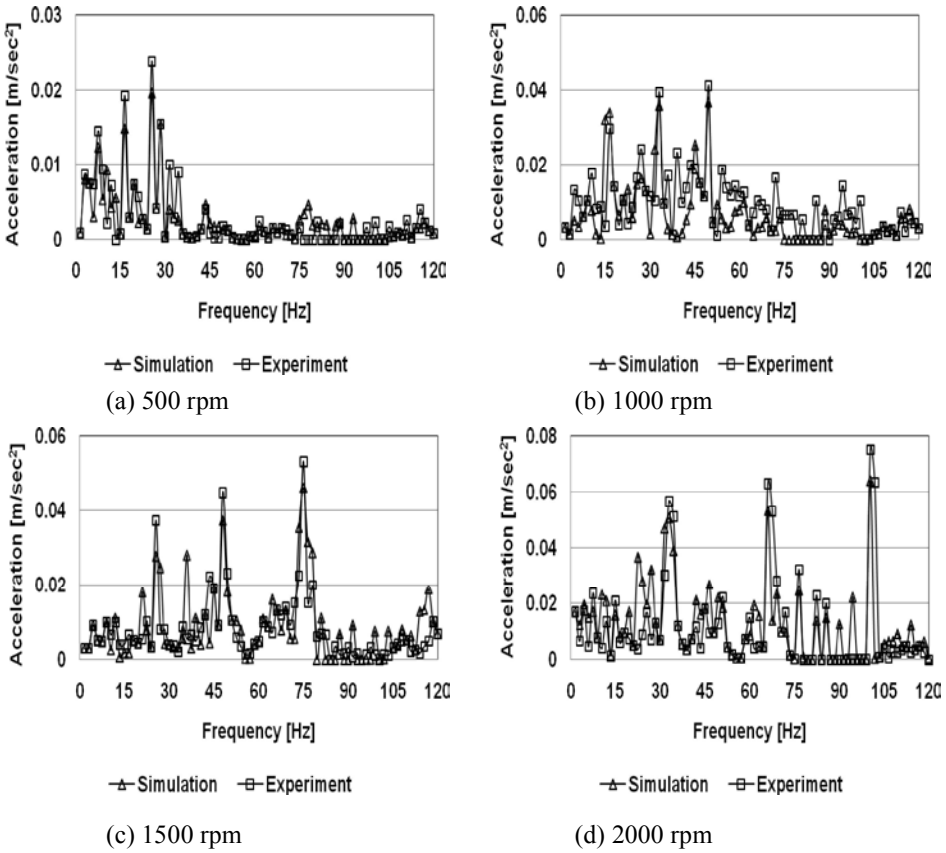

Fig. 6: Base line spectrum of Drive End at different speeds

Table 4: Comparisons of vibration amplitudes of base line signal

	Experimental value in m/sec²						Simulation value in m/sec²					
	DE			NDE			DE			NDE		
RPM	1X	2X	3X	1X	2X	3X	1X	2X	3X	1X	2X	3X
500	0.012	0.015	0.019	0.049	0.032	0.066	0.013	0.019	0.024	0.045	0.024	0.049
1000	0.040	0.036	0.037	0.046	0.044	0.042	0.029	0.039	0.041	0.023	0.029	0.024
1500	0.028	0.037	0.529	0.037	0.044	0.053	0.037	0.045	0.053	0.027	0.037	0.046
2000	0.051	0.053	0.064	0.063	0.068	0.074	0.041	0.063	0.075	0.046	0.053	0.064

coupling at four speeds 8.33 Hz, 16.67 Hz, 25 Hz and 33.333 Hz (500, 1000, 1500, 2000 rpm) shown in Figure 6 and 7. The base line spectrum is measured experimentally using dual channel vibration analyzer. The same shaft with coupling and bearing is modeled and simulated using ansys and the vibration amplitudes are measured at DE and NDE at four speeds as measured in experiment. Table 4 shows the experimental and simulated vibration amplitudes in m/sec^2 of base line condition at both DE and NDE.

Figure 6 (a) to (d) shows the DE frequency spectrum of both experimental and simulated results at different speeds. The maximum vibration amplitude of 0.064 m/sec^2 and 0.075 m/sec^2 is observed in experiment and simulation at 3X of 2000 rpm. Peak vibration amplitude values of very small magnitude are observed at other speeds. At lower speed the vibration amplitude is very small. From Figure 7 (a) to (d) also it is observed that both experimental and simulation vibration amplitudes of NDE at different speeds are very close agreement

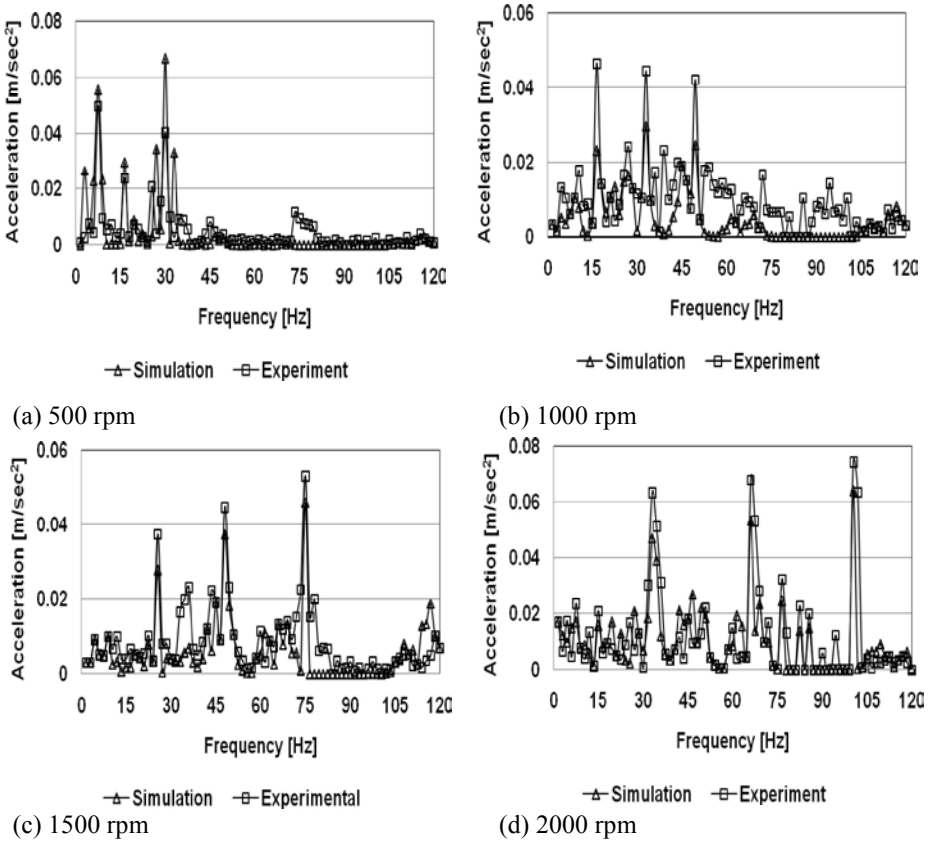

Fig. 7: Base line spectrum of Non Drive End at different speeds

Table 5: Comparisons of vibration amplitudes of unbalanced signal (Unbalanced mass of 18 gram)

	Experimental value in m/sec²						Simulation value in m/sec²					
	DE			NDE			DE			NDE		
RPM	1X	2X	3X	1X	2X	3X	1X	2X	3X	1X	2X	3X
500	0.031	0.016	0.016	0.025	0.008	0.020	0.028	0.003	0.001	0.020	0.003	0.015
1000	0.047	0.016	0.042	0.056	0.011	0.025	0.041	0.001	0.033	0.029	0.007	0.025
1500	0.054	0.015	0.050	0.037	0.014	0.032	0.054	0.009	0.040	0.030	0.002	0.020
2000	0.097	0.029	0.081	0.067	0.022	0.048	0.074	0.004	0.061	0.062	0.002	0.048

with each other. Maximum vibration amplitude of 0.074 m/sec^2 and 0.064 m/sec ^{2}at 3X of 2000 rpm is observed in experiment and simulated respectively. Small amount of peaks at harmonics of shaft speed are the indication of manufacturing errors of coupling and other elements like rubber pad or rubber bush that cannot be eliminated. From the vibration spectrum of both DE and NDE it is also observed that newly designed pin type coupling produce very little amount of vibration at different speeds. So it is concluded that, the newly designed coupling is to withstand without much vibration at different speeds. Experimental amplitudes are very close to the simulation amplitudes. Hence, good alignment is noticed from the frequency spectrum.

Frequency Spectrum of Unbalance of 18 Gram at a Radius of 54 Mm in Overhang Rotor: The unbalance is created by placing mass of 18g at the overhung rotor at a radius of 54 mm. The experiment is repeated with misaligned condition. Signals are measured again at the same four speeds as mentioned above. Vibration signals are acquired at both the drive end and non-drive end and recorded in the analyzer. Table 5 shows the experiment

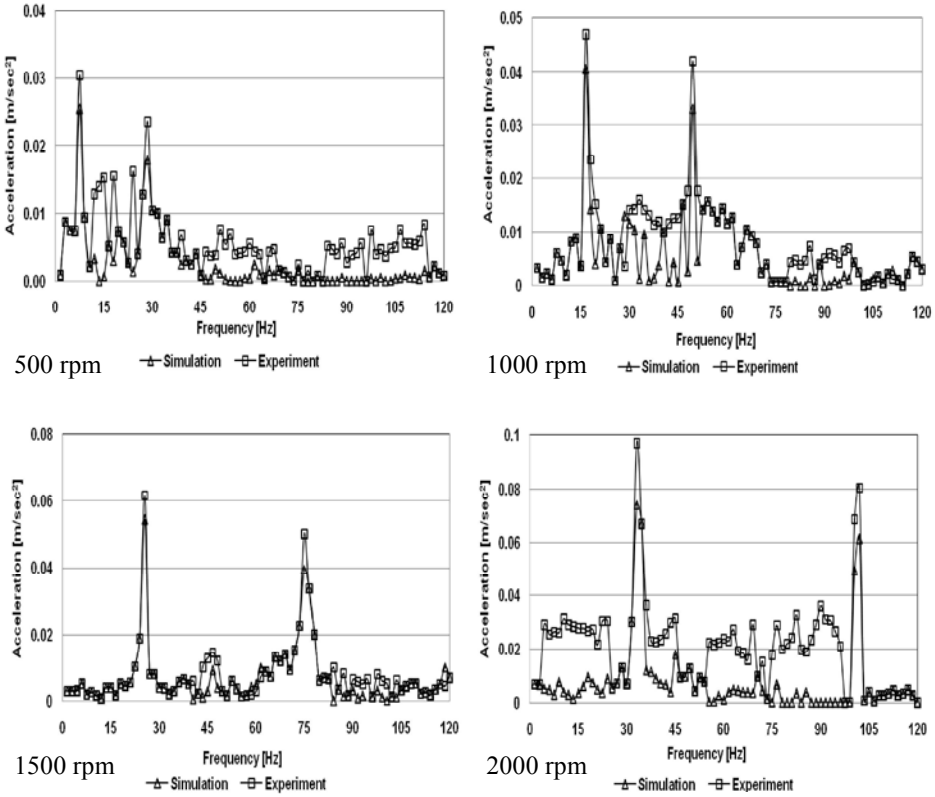

Fig. 8: Unbalanced spectrum of Drive End at different speeds

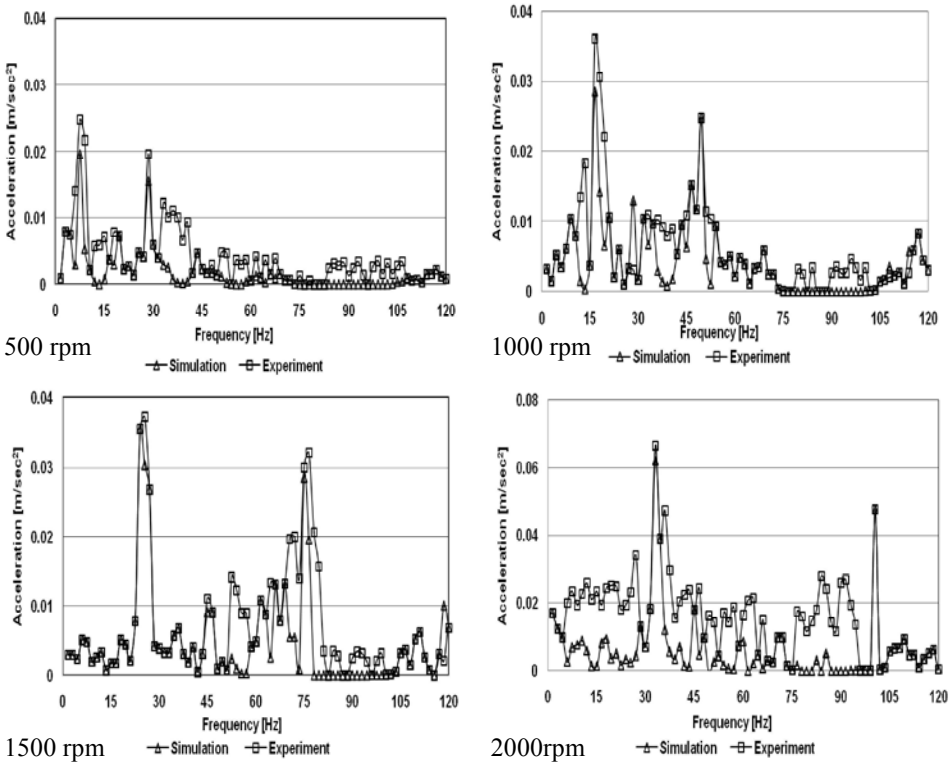

Fig. 9: Unbalanced spectrum of Non Drive End at different speeds

Table 6: Percentage increase in Amplitude

	% Increase in Amplitude			
	Experimental		Simulation	
Speed	DE	NDE	DE	NDE
500	2.58	0.78	2.15	0.44
1000	1.18	1.21	1.41	1.26
1500	1.93	1.00	1.46	1.10
2000	1.90	1.06	1.81	1.34

and simulation vibration amplitude in m/sec^2 of both DE and NDE at different speeds. The experimental and numerical frequency spectra of DE and NDE for the unbalanced condition are shown in Figure 8 and Figure 9. From Figure 8 (a) to (d), at 500 rpm, maximum vibration amplitude of 0.031 m/sec^2 and 0.028 m/sec^2 noticed in experiment and simulation respectively at DE. Frequency of the maximum amplitude is at 7.5 Hz which is first harmonic of running speed. At 500 rpm the vibration amplitude is 2.58 times and 2.15 times more than the base line vibration at first harmonic (1X) frequency in experiment and simulation respectively. The increase in amplitude at 1X frequency indicates the presence of unbalance in the shaft. Similarly all other speeds maximum vibration amplitude obtained at first harmonics (1X). Both DE and NDE frequency spectrum shown in Figure 8 and 9 are indicates that the first harmonics (1X) has the peak value in all speeds. This is the good indicator of the shaft unbalance. Table 6 shows the percentage of increase in amplitude of different speeds at both DE and NDE of the experiment and simulation spectrum. From the Table 6 It is clearly understood that, when unbalanced shaft speed increases vibration amplitude is also increases. The newly designed 3 pin type coupling has a very little amount of vibration during the unbalanced condition. So the designed coupling is rigid and able to withstand at higher speeds without much vibration.

CONCLUSION

The model of the pin type coupling-ball bearing system with unbalance was simulated. Throughout the experimental and simulation works, the validity of the model was successfully verified and the rotor dynamic characteristics related to unbalance were investigated. The experimental and simulated frequency spectra were obtained. The experimental predictions are in good agreement with the ansys results. Both the experiment and simulation results spectra shows that unbalance can be characterized primarily first harmonic (1X) of shaft running speed. However, unbalance (1X shaft running speed) effect is not close enough to one of the system natural frequencies to excite the system appreciably. Therefore in some case the unbalance response is hidden and does not show up in the vibration spectrum. On the other hand, if 1X shaft running speed is at or close to one of the system natural frequencies, the unbalanced effect can be amplified and a high acceleration level at 1X shafts running speed is pronounced in the frequency spectrum.

As the speed increases the amplitude at 1X is also increases for the same unbalance weight. This increase in value is because of the different unbalanced force. The drive end amplitude is slightly more or less than the non drive end magnitude. This indicates that the overhung rotor is very near the non drive end and vibration level is very high in this bearing. This phenomenon can be used in predictive maintenance to monitor the unbalance conditions. Existence of unbalance in rotating system with overhung rotors is closely related to two important signatures. First the 1X radial acceleration spectrum magnitude and the other more significantly and strongly related to non-drive end (the one close to the overhung rotor) bearing vibration amplitude.

REFERENCE

1. Eshleman, R. And A. Eubanks, 1969. “On the critical speeds of a continuous rotor”, J. Engineering for Industry, 91: 1180-1188.
2. Mitchell, L. And D.D.M. Mellen, 1995. “Torsional-lateral coupling in a geared high-speed rotor system”, ASME Design Engineering Technical Conferences 3 (Part B), 84(2): 977-989.
3. Lee, J.W. and D.H. Ha, 2003. “Choi, Coupled lateral and torsional vibration characteristics of a speed increasing geared rotor-bearing system”, J. Sound and Vibration, 263(4): 725-742.

4. Rao, J.S. Chang and T.N. Shiau, 1995. "Coupled bending-torsion vibration of geared rotors", ASME Design Engineering Technical Conferences 3(Part B), 84-2: 977-989.
5. Neriya, R.B. Bhat and T.S. Sankar, 1985. "Coupled torsional flexural vibration of a geared shaft system using finite element method", The Shock and Vibration Bulletin (Part 3), 55: 13-25.
6. Kahraman, H.N., Ozguven, D.R. Houser and J.J. Zakrajsek, 1992. "Dynamic analysis of geared rotors by finite elements", Transactions J. Mechanical Design, 114: 507-514.
7. Iida, A. Tamura, K. Kikuch and H. Agata, 1980. "Coupled torsional-flexural vibration of a shaft in a geared system of rotors (1st report)", Bulletin of the JSME, 23(186): 2111-2117.
8. Iwatsubo, S. Arii and R. Kawai, 1984. Coupled lateral-torsional vibration of rotor system trained by gears", Bulletin of JSME, 27(224): 271-277.
9. Choi, S.Y. Mau, 1995. "Dynamic analysis of geared rotor-bearing systems by the transfer matrix method", ASME Design Engineering Technical Conferences 3 (Part B), 84: 2967-2976.
10. Hibner, 1975. "Dynamic response of viscous-damped multi-shaft jet engines", J. Aircraft, 12(4): 305-312.
11. Li, L. Yan and J.F. Hamilton, 1986. "Investigation of the steady-state response of a dual-rotor system with inter shaft squeeze film damper", Transactions J. Engineering for Gas Turbines and Power, 108: 605-612.
12. Gupta, K.D. Gupta and K. Athre, 1993. "Unbalance response of a dual rotor system: theory and experiment", Transactions J. Vibration and Acoustics, 115: 427-435.
13. Rao, J.S., 1996. "Rotor Dynamics, 3rd edition, New Age International Publishers, India.
14. Rao, T.N. Shiau and J.R. Chang, 1998. "Theoretical analysis of lateral response due to torsional excitation of geared rotor", Mechanism and Machine Theory, 33(6): 761-783.
15. Shiau, J.S. Rao, J.R. Chang and S.T. Choi, 1999. Dynamic behavior of geared rotors, Transactions J. Engineering for Gas Turbine and Power, 121: 494-503.
16. Lee, Y.S. Lee, 2001. Rotordynamic characteristics of an APU gas turbine rotor-bearing system having a tie shaft, KSME Intl. J., 15(2): 152-159.